The stoichiometry of the structure may be deduced from Fig. 5 by assuming that Ga occupies the edge-shared octahedral and the tetrahedrally coordinated sites characteristic of β-gallia, that Ti occupies the octahedrally coordinated sites in the rutile-like columns, and that Ba occupies the eight-coordinated sites in the hollandite-like tunnels. For tunnel occupancy $\frac{1}{2}$ we obtain $BaTi_6Ga_{12}O_{31}$, assuming all cations have maximum oxidation states. However, we note that, in general, Ti may substitute for Ga in the edge-shared octahedral sites so that if the tunnel occupancy (x) is allowed to vary we obtain $Ba_xTi_{8-2x}Ga_{10+2x}O_{31}$, where the maximum extent of x is $0{\cdot}0 < x < 2{\cdot}0$. Further studies of the stabiility range of this phase, and of any possible ordering of Ba along the tunnels (*i.e.* along **c**), and of the isomorphous phase $Ba_xTi_{8-x}Mg_{10+x}O_{31}$, are in progress.

This work was financially supported by the Australian Research Grants Committee and the University of Melbourne. The assistance of Mr R. Glaisher, with the image calculations, is gratefully acknowledged.

References

BURSILL, L. A. (1979*a*). *Acta Cryst.* B**35**, 530–538.

BURSILL, L. A. (1979*b*). *Acta Cryst.* A**35**, 449–458.

BURSILL, L. A. (1979*c*). *Direct Imaging of Atoms in Crystals and Molecules*. Nobel Symp. No. 47, Lidingo; *Chem. Scr.* **14**, 83–97.

BURSILL, L. A. & GRZINIC, G. (1980). *Acta Cryst.* B**36**, 2902–2913

BURSILL, L. A., SPARGO, A. E. C., WENTWORTH, D. & WOOD, G. J. (1979). *J. Appl. Cryst.* **12**, 279–286.

BURSILL, L. A. & WILSON, A. R. (1977). *Acta Cryst.* A**33**, 672–676.

COWLEY, J. M. (1975). *Diffraction Physics*, p. 60. New York: North-Holland.

LYNCH, D. F., MOODIE, A. F. & O'KEEFE, M. A. (1975). *Acta Cryst.* A**31**, 300–307.

MACLAGAN, D. S., BURSILL, L. A. & SPARGO, A. E. C. (1977). *Philos. Mag.* **35**, 757–780.

SCHERZER, O. (1949). *J. Appl. Phys.* **20**, 20–29.

SPENCE, J. H. C., O'KEEFE, M. A. & IIJIMA, S. (1978). *Philos. Mag.* **38**, 463–482.

SPENCE, J. H. C., O'KEEFE, M. A. & KOLAR, J. (1977). *Optik*, **49**, 307–323.

WILSON, A. R., BURSILL, L. A. & SPARGO, A. E. C. (1979). *Optik*, **52**, 313–336.

Acta Cryst. (1980). B**36**, 2902–2913

Incommensurate Superlattice Ordering in the Hollandites $Ba_xTi_{8-x}Mg_xO_{16}$ and $Ba_xTi_{8-2x}Ga_{2x}O_{16}$

BY L. A. BURSILL* AND G. GRZINIC

Department of Physical Chemistry, Lensfield Road, Cambridge CB2 1EP, England

(*Received* 17 *December* 1979; *accepted* 15 *August* 1980)

Abstract

Electron diffraction studies revealed a continuous variation of superlattice periodicity $m \times d_{002}$ with changes in stoichiometry x of the hollandite phases $Ba_xTi_{8-x}Mg_xO_{16}$ and $Ba_xTi_{8-2x}Ga_{2x}O_{16}$ with $4{\cdot}70 < m < 5{\cdot}93$ for $0{\cdot}80 < x < 1{\cdot}33$. The superlattice only becomes commensurate for $x = 1{\cdot}20$ ($m = 5{\cdot}00$). High-resolution (3 Å) electron microscope images and computer-simulation techniques were used to determine the short-range ordered arrangements of Ba^{2+} ions within the tunnels of the MX_2 framework of the hollandite structure. Three basic structures were found, for $x = 0{\cdot}80$, $1{\cdot}20$ and $1{\cdot}33$, and the incommensurate periodicities explained in terms of intergrowths of these three plus small elements of an $m = 2$ structure. The origin of the range of incommensurate spacings is discussed in terms of electrostatic repulsions between Ba^{2+} ions and the observed softening of the A_5 transverse acoustic mode of rutile (TiO_2) for $m = 6$. Diffusion mechanisms for ionic conductivity in hollandites are briefly discussed but it is clear that the observations and analysis presented here explain why hollandites gave very disappointing results when used as solid electrolytes even though dielectric measurements suggested a relatively low activation energy ($0{\cdot}17$ eV) for Ba^{2+} ion hopping. In fact the structural models used previously and the corresponding interpretations of dielectric absorption measurements were based on oversimplifications of the real structures.

* On leave from: School of Physics, The University of Melbourne, Parkville, Victoria 3052, Australia.

0567-7408/80/122902-12$01.00

1. Introduction

Hollandite-type phases are of current interest for their possible value as solid electrolytes or electrode materials (Rean, Delmas & Hagenmuller, 1978; Boyce & Huberman, 1979). On the other hand, it has been suggested that tunnels in the structure (Fig. 1) may stably incorporate radioactive ions such as Na, K, Rb, Cs, Ba, Sr and Pb. Ringwood (1978) suggested that radioactive Cs be incorporated in the solid solution $Cs(Al,Fe)Ti_3O_8/Ba_{0.5}AlTi_3O_8$, whereby the Ba^{2+} ions, replacing monovalent Cs^+, will 'lead to a strengthening of the structure, decreasing its leachability'. It seems to us that the requirements of high ionic mobility, for a solid electrolyte, and for geologically stable structures for safe radioactive-waste disposal, are diametrically opposed. It is therefore necessary to examine the distribution of various mono- and divalent ions in the tunnels of the hollandite phase. Earlier we have investigated the structural relationships between the rutile (TiO_2), β-gallia (Ga_2O_3) and hollandite phases (Bursill, 1979*a*,*b*) and have established the electron optical requirements for direct imaging of the Ba^{2+} ions in the *c*-axis projection of the structure (Bursill & Wilson, 1977).

Single-crystal X-ray diffraction studies of the phase $Ba_xMg_xTi_{8-x}O_{16}$, $0{\cdot}67 < x < 1{\cdot}14$, showed it to be tetragonal with unit-cell parameters $a_1 = a_2 = 10{\cdot}110$, $c = 2{\cdot}986$ Å (Dryden & Wadsley, 1958). The fractional coordinates were essentially identical to those reported earlier for the hollandite group of minerals (Byström & Byström. 1950). Dryden & Wadsley also reported additional diffuse reflections having positions and intensities which were thought to be independent of chemical composition in the range $0{\cdot}67 < x < 1{\cdot}14$. At $x = 1{\cdot}0$ strong dielectric absorption was found parallel to the tunnel direction (Fig. 1). They proposed that each Ba^{2+} site has fractional occupancy $\frac{1}{2}$ for $x = 1$. At $x = 0{\cdot}67$ the ratio of the Ba^{2+} to vacant tunnel sites is 1:2 but the dielectric absorption was virtually unchanged. It was therefore suggested that the sequence Ba^{2+}–vacancy–Ba^{2+}–vacancy must now be present along a certain fraction of the tunnels, giving unchanged dielectric absorption, but that the remaining tunnels should contain long strings of empty sites, or else be completely empty. Thus the nonstoichiometric phase $Ba_xTi_{8-x}Mg_xO_{16}$ should contain varying ratios of filled to empty tunnels for $0{\cdot}67 < x < 1{\cdot}0$. Presumably for $1{\cdot}0 < x < 1{\cdot}14$ the fractional occupancy of each tunnel site would gradually increase from $\frac{1}{2}$ to 0·67. In order to explain the almost structureless diffuse sheets in the diffraction pattern it was proposed that the sequences in adjacent tunnels are not correlated in phase.

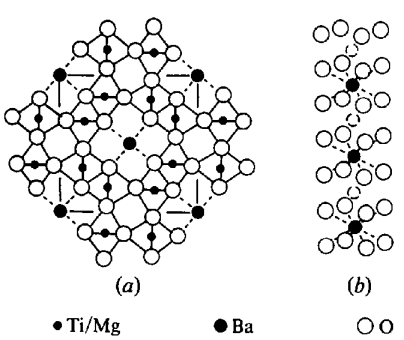

Fig. 1. (*a*) The hollandite structure in [001] projection. $[MO_6]$ octahedra share edges along the projection axis, forming strings which are linked by corner-sharing and edge-sharing to form square tunnels which contain Ba^{2+} ions in cubic coordination. (*b*) Cubic coordinated Ba^{2+} sites sharing faces along [001]. Filled and dotted circles indicate the sequence Ba^{2+}–vacancy–Ba^{2+}–vacancy of filled and empty sites as expected intuitively for $Ba_{1.0}Mg_{1.0}Ti_{7.0}O_{16}$. The large open circles indicate O atoms which are part of the framework shown in (*a*).

Beyeler (1976) reported diffuse supplementary scattering in a hollandite of stoichiometry $K_{1.54}Mg_{0.77}Ti_{7.23}O_{16}$ which had approximately $\frac{3}{4}$ of the cubic coordinated tunnel sites filled. A diffuse sheet was situated 0·22 reciprocal-lattice units (1 r.l.u. = $2{\cdot}90^{-1}$ Å^{-1}) from the Bragg spots, corresponding to a multiplicity of $m = 4{\cdot}55$ along $k(001)$. These sheets had a width of approximately 0·08 r.l.u., which corresponds to a correlation length of 35 Å, *i.e.* 12 tunnel sites. The diffuse intensity was analysed in terms of a supercell containing four sites, one of which was assumed to be empty, and the adjacent K^+ ions were given fractional displacement u towards the empty sites. Again it was assumed that sequences in adjacent tunnels suffer random phase shifts. The intensity of the diffuse scattering was sensitive to u and on comparison with experiment, after allowing an admixture of sequences of length 4 and 5 times *c*, a value of $u = 0{\cdot}245$, *i.e.* 0·71 Å was obtained. The K^+ hollandite phase apparently exists over the range $1{\cdot}5 < x < 2{\cdot}0$ (Beyeler, 1976) but no measurements of the variation of superlattice multiplicity m or K^+-ion displacement u were reported.

In this paper we report the results of a high-resolution (3 Å) imaging and electron diffraction study of $Ba_xTi_{8-x}Mg_xO_{16}$ and $Ba_xTi_{8-x}Ga_{2x}O_{16}$ ($0{\cdot}8 < x < 1{\cdot}33$) which shows that the structural model proposed by Dryden & Wadsley and their interpretation of the dielectric absorption results represent an oversimplification of the real situation. In fact, there are very strong correlations between the ordering in adjacent tunnels, the positions of the superlattice reflections are very well defined in the Ba hollandites and vary continuously with stoichiometry (x), and there is no evidence for emptying of a fraction of the tunnels as x decreases. Nevertheless, the real structure is entirely consistent with the dielectric measurements. Our evidence for strong short-range-order correlations and a microdomain texture perhaps explains why hollandites are not such useful solid electrolytes as may have been intuitively envisioned. Furthermore, the

strong electrostatic repulsions between Ba^{2+} ions, which presumably underlay the ordering patterns observed, do suggest that hollandite phases should be further investigated for possible use for stable storage of radioactive waste.

2. Experimental

Samples of $Ba_xTi_{8-x}Mg_xO_{16}$ and $Ba_xTi_{8-2x}Ga_{2x}O_{16}$ were prepared by reacting weighed amounts of $BaCO_3$, TiO_2, Ga_2O_3 and MgO powders (Koch-Light, 4N). The mixtures were pelletized and sealed in 3 mm diameter platinum tubes. These were then reacted at temperatures ranging from 1373–1573 K for periods varying from a few hours to 4 weeks. Initially the samples were removed from the furnace and left to cool in air, reaching room temperature after several minutes (~5 min). Later, more homogeneous products were obtained by first melting the pellets, inside the Pt tubes using a H_2/O_2 torch, before annealing in the furnace as before. Significant improvement in the sharpness of the superlattice reflections was then achieved by slow cooling of the reacted specimens from 1273, 1073, 800 and 673K. The samples were examined optically for homogeneity and colour. Mostly fine-grained white polycrystalline masses were obtained. However, if some reduction occurred, or if the tube was inadvertently opened to the atmosphere inside the furnace, darkish coloured products were obtained. The latter were discarded for the present study.

Fragments of the preparations were then ground under chloroform, in an agate mortar and pestle, and deposited onto carbon-lace support film. The thin edges were examined using a high-tilt side-entry goniometer allowing [100] or [010] and [001] zone diffraction patterns to be obtained from the same area. This allowed the superlattices to be unambiguously identified. Selected specimens were then examined in a Jeol 100C electron microscope fitted with ultra-high-resolution objective-lens pole-pieces and a specially constructed goniometer (Bursill, Spargo, Wentworth & Wood, 1979). The electron optical parameters are: spherical-aberration coefficient $C_s = 0{\cdot}7$ mm, chromatic aberration $C_c = 1{\cdot}05$ mm, and focal length $f_o = 1{\cdot}35$ mm. Crystals were tilted into the [100] zone in order to display best the superlattice ordering along the c axis, *i.e.* along the tunnels. Images were recorded at magnifications of 330 000× to 1 000 000×, using objective-lens defocus values -200 Å $< \Delta f < -1000$ Å and focused illumination (semi-cone angle $\alpha \sim 0{\cdot}8$–$1{\cdot}0$ mrad). Under these conditions this lens should allow 'structure images' to be obtained at approximately 2·9 Å resolution, point-to-point, provided the crystals are sufficiently thin (see, for example, Bursill & Wood, 1978; Bursill, 1979*c*, 1980).

3. Results

(*a*) *Electron diffraction analysis of superstructures*

Fig. 2(*a*,*b*,*c*,*d*) shows [100] zone electron diffraction patterns of samples having $x = 0{\cdot}8$, $1{\cdot}0$, $1{\cdot}2$ and $1{\cdot}33$ respectively. Note that the superlattice multiplicity m varies from 4·75 to 5·86. The superlattice intensities are sharp and in striking contrast to the X-ray photograph for $K_{1.54}Mg_{0.77}Ti_{2.23}O_{16}$ (Beyeler, 1976, Fig. 1). Note that $x = 1{\cdot}0$ exhibits $m = 4{\cdot}81$, not $m = 2$ as would be expected intuitively using Wadsley's Ba^{2+}–vacancy–Ba^{2+}–vacancy model. The superlattice only becomes commensurate for $x = 1{\cdot}2$, when $m = 5{\cdot}0$. A large number of patterns have been obtained for intermediate compositions and it is clear that there is a continuous change in m corresponding to changes in x in the range $0{\cdot}8 < x < 1{\cdot}33$ with $4{\cdot}70 < m < 5{\cdot}93$. So far we have not succeeded to make $m > 6{\cdot}00$ in the Ba/Mg or Ba/Ga systems. For preparations having $x > 1{\cdot}33$ we find $m < 5{\cdot}8$–$5{\cdot}9$ coexisting with another as yet unidentified phase. Similarly for $x < 0{\cdot}8$ we find $m \sim 4{\cdot}70$ coexisting with a phase exhibiting either pure rutile (TiO_2) type diffraction patterns or sometimes the gallium titanate structures $Ga_4Ti_{m-4}O_{2m-2}$ ($m \sim 20$). The [001] zone axis diffraction patterns always show sharp spots having the square net characteristic of hollandite (Fig. 3). Our experiments with sealed tubes always yielded samples containing this simple c-axis diffraction pattern. [We wish to note, however, that we have found evidence for small departures from orthogonality of the a_1 and a_2 axes, for $2a_1 \times 2a_2$ and $a_1 \times 2a_2$ superstructures for samples prepared in open platinum boats. The origin of these superstructures is still under investigation (L. A. Bursill, G. Grzinic and D. J. Netherway, in preparation) but it appears to be due to the inadvertent substitution of Al^{3+} ions into the structure.]

So far we have not clearly established significant differences between the diffraction patterns of the Ba/Mg and Ba/Ga hollandite having the same values of x. There may be some differences in the extreme values of the multiplicity m and in its temperature variation, but these have not yet been measured.

(*b*) *High-resolution images of the* [100] *zone*

Fig. 4(*a*,*b*,*c*,*d*) shows high-resolution (~3 Å) images, corresponding to $x = 0{\cdot}8$, $1{\cdot}0$, $1{\cdot}2$ and $1{\cdot}33$. The important contrast features are the rows of bright blobs, separated by lines of dark intensity, parallel to the c axis, *i.e.* along the tunnels. Inspection of Fig. 4(*a*) ($x = 0{\cdot}8$, $m = 4{\cdot}75$) reveals patches (or domains) of diameter approximately 20–60 Å containing regular arrangements of blobs. These show two blob spacings along the tunnel direction (c). The first are approximately $2c$ (6 Å) which are clearly resolved and the

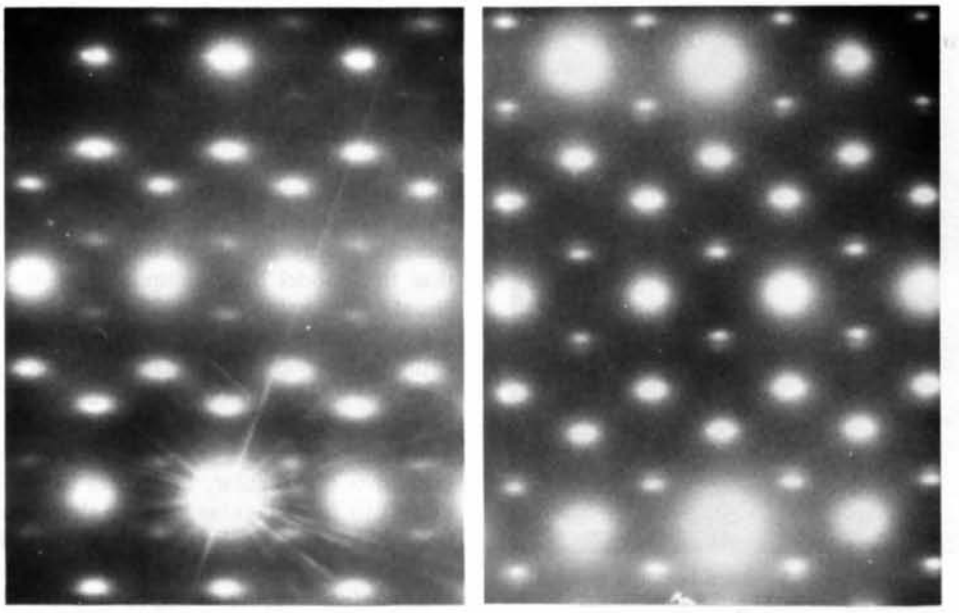

(*a*) ($m = 4{\cdot}75$)

(*b*) ($m = 4{\cdot}81$)

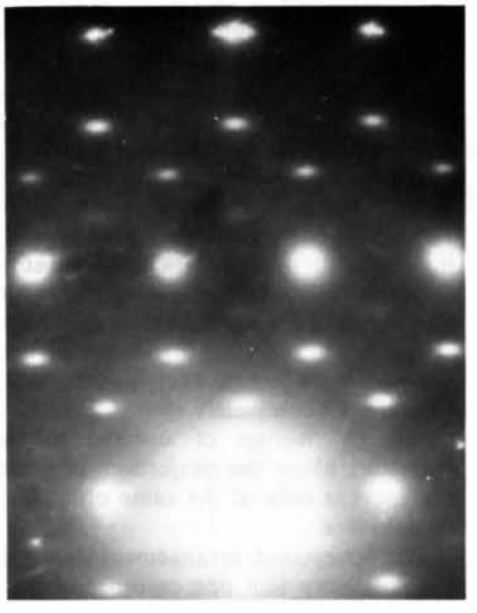

(*c*) ($m = 5{\cdot}06$)

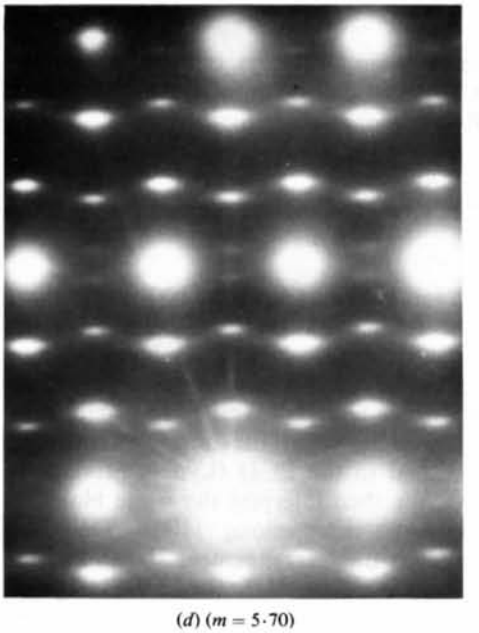

(*d*) ($m = 5{\cdot}70$)

Fig. 2. (*a*),(*b*),(*c*),(*d*) The [100] zone electron diffraction pattern of $Ba_xTi_{8-2x}Ga_{2x}O_{16}$ samples with $x = 0{\cdot}8$, $1{\cdot}0$, $1{\cdot}2$ and $1{\cdot}33$ respectively. Note superlattice multiplicity (m) varies continuously with $4{\cdot}75 < m < 5{\cdot}86$. The superlattice is commensurate (m integral) only for $x = 1{\cdot}20$.

second are approximately 3 Å, which are mostly just resolved in this case. The former pairs of blobs tend to show very uniform intensity whereas for the latter one or other of the blobs is often of much lower intensity. Inspection of Fig. 4(*c*) ($m = 5$) also shows domains having a regular blob arrangement. In this case a regular honeycomb array occurs. Similarly, Fig. 4(*b*) shows elements common to both $x = 0{\cdot}8$ and $x = 1{\cdot}2$ structures. In addition, zigzag arrays of blobs occur in all of Figs. 4(*a*,*b*,*c*). Fig. 4(*d*) ($x = 1{\cdot}33$) shows a third type of regular arrangement consisting essentially of zigzag arrays of white blobs separated by 3*c* (approximately 9 Å). In this paper we will concentrate on analysing the regular structures which appear at different stoichiometries. Other micrographs, for x values in between $x = 0{\cdot}8$, $1{\cdot}2$ and $1{\cdot}33$, show

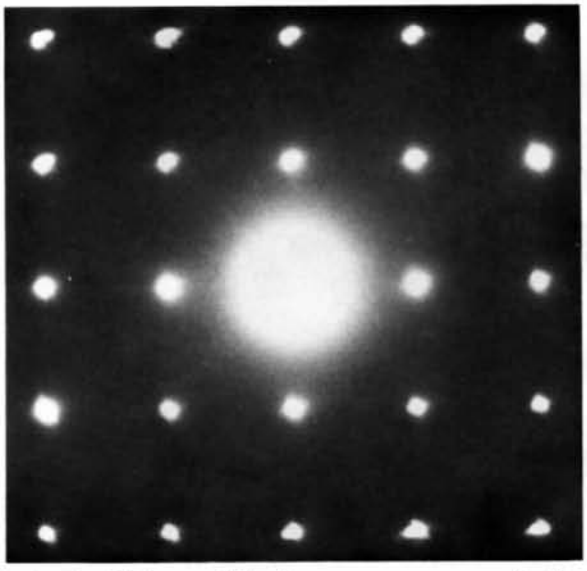

Fig. 3. The [001] zone diffraction pattern common to $Ba_xTi_{8-x}Mg_xO_{16}$ and $Ba_xTi_{8-2x}Ga_{2x}O_{16}$ ($0{\cdot}8 < x < 1{\cdot}33$).

mixtures of these basic structures (already evident in Fig. 4*a*,*b*,*c*,*d*). Detailed discussion of these intergrowth structures will be left for a later paper.

4. Derivation of structural models for ordering of Ba^{2+} ions

The ideal Ba^{2+} ion positions for the [100] projection, based upon the framework structure determined by Dryden & Wadsley (see also Byström & Byström), are drawn in Fig. 5. At this stage it is convenient to assume that the projected-charge-density approximation (PCDA) is applicable, when the image intensity is directly proportional to the PCD (Lynch, Moodie & O'Keefe, 1975). We then interpret the white blobs as indicating empty Ba sites along [100]. Thus we deduced the ordered Ba^{2+} arrangement shown in Fig. 6(*a*) from the regular domains shown in the image of Fig. 4(*a*). In fact this simple PCDA is unlikely to be satisfied in reality. It is very common to find, from analysis of computer simulations using the full *N*-beam dynamical multislice techniques, that sequences of different images are obtained as Δf or H vary. These typically involve some images superficially resembling the PCDA. However, in general, contrast reversals may occur or the image may shift by some fraction of a lattice vector relative to the 'PCD' image. For special values of H and Δf blobs splitting may occur. None of these effects are predicted by the PCDA. Thus in general there is a homomorphism (many-to-one correspondence) between white/or dark blobs in the image and the PCD (Bursill, 1979*c*). For ordered structures this homomorphism is often sufficient to allow the structure to be visualized, with some limited degree of resolution. Having deduced a structural model it is then necessary to carry out full-scale multislice calculations to confirm the structure by image matching over a range of Δf and H values (see §5). The model deduced in Fig. 6(*a*) clearly reproduces the pattern of white blobs observed in Fig. 4(*a*); open and filled circles indicate empty and filled Ba^{2+} sites respectively. Note that this model has multiplicity $m = 5$, which is not equal to the value $m = 4{\cdot}75$ found for the corresponding diffraction pattern (*cf.* Fig. 2*a*). This discrepancy is explained by observing that defects occur in the image (Fig. 4*a*) which corresponds to intergrowth of domains of $m = 5$ structure with small elements of an $m = 2$ hollandite structure indicated in Fig. 6(*b*). The intergrowth is not regular, *i.e.* the $m = 2$ elements do not extend to form regular lines or slabs. An admixture of only 8% of $m = 2$ is required to reduce the mean multiplicity m from 5·0 to 4·75. This corresponds to a mean defect spacing of approximately 40 Å along each tunnel. Assuming $x = 1$ for the $m = 2$ regions we find the mean stoichiometry shifts from $x = 0{\cdot}800$ for $m = 5$ to $x = 0{\cdot}807$ for $m = 4{\cdot}75$. It is significant that preparations having $x \leq 0{\cdot}8$ contain rutile (TiO_2) as a second phase. Thus the lower limit of the Ba hollandite phase is deduced to be $x = 0{\cdot}80$, in disagreement with Dryden & Wadsley's value of $x = 0{\cdot}67$. However, we note that this value refers to preparations reached at 1473 K and slow cooled. It is possible this limit will be shown to be temperature-dependent and differ depending on the di- or trivalent cations substituted for Ti^{4+} in the MX_2 hollandite framework. For example, $m = 4{\cdot}65$ was obtained for one Ba/Ga sample having an overall $x = 0{\cdot}50$. The varying brightness of the closer-spaced pairs of blobs in Fig. 4(*a*) suggests that some of these sites are not completely empty. This may simply correspond to overlap of ordered domains (20–60 Å diameter) along the projection axis, since the crystal thickness is only of the same order (say 60 Å) as the domain size.

The honeycomb arrangement shown in Fig. 6(*a*) and the possibility that one or other of the empty pair of Ba^{2+} sites may be fractionally occupied leads naturally to models for the commensurate superlattice and regular honeycomb arrangement of white blobs found for $x = 1{\cdot}2$ ($m = 5$) (Fig. 4*c*). Fig. 7 shows three possible $m = 5$, $x = 1{\cdot}2$ structures. The first two (*a*,*b*) are symmetrically equivalent ordered patterns, obtained from the $x = 0{\cdot}8$ structure by assuming full occupancy of one or other of the closely spaced pair of sites. The third (*c*) corresponds to a disordered structure with fractional occupancy $\frac{1}{2}$ for each of this pair of sites. Elements of all three of these proposed structures appear in Fig. 4(*c*) and it is again necessary to involve a microdomain model with short-range-order correlations to explain even the commensurate $m = 5$ structure.

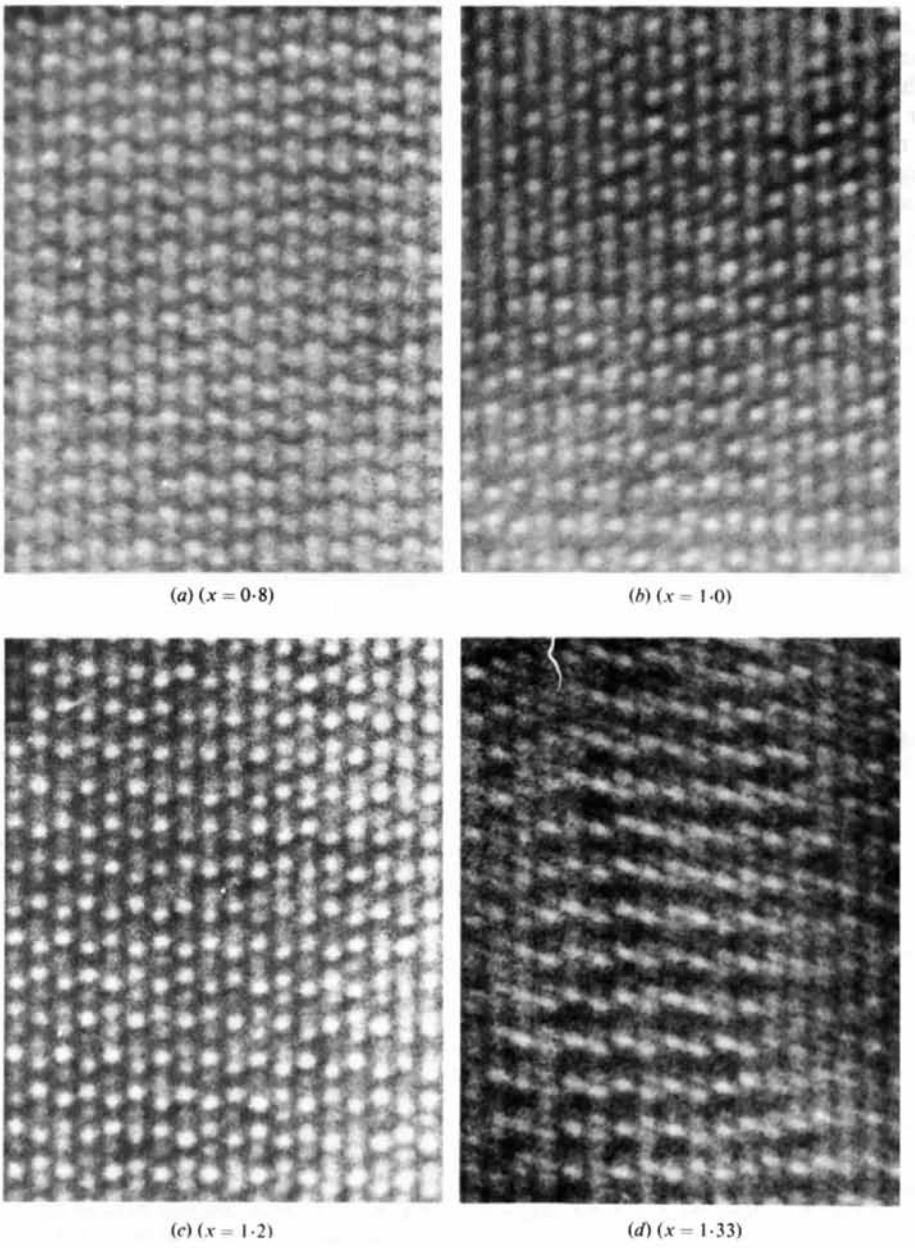

(*a*) ($x = 0{\cdot}8$) (*b*) ($x = 1{\cdot}0$)

(*c*) ($x = 1{\cdot}2$) (*d*) ($x = 1{\cdot}33$)

Fig. 4. (*a*),(*b*),(*c*),(*d*) High-resolution images for $x = 0{\cdot}8$, $1{\cdot}0$, $1{\cdot}2$ and $1{\cdot}33$ respectively with the [100] zone. Note the rows of white blobs parallel to the tunnel direction [001]. The predominant blob spacings are 6 and 3 Å in (*a*), 6 and 9 Å in (*c*) and 9 Å in (*d*). Small ordered regions ~20–60 Å in diameter may be located by sighting along different lattice directions.

Note, however, that in this case it is not necessary to have composition variations. A large variety of cooling rates was used in an attempt to induce ordering over large volumes. In fact, Fig. 4(*c*) represents one of the better ordered preparations.

It is clear that the essential framework of the hollandite structure must now be extended from the $[MO_6]$ octahedral linkages to include (for $0{\cdot}8 < x < 1{\cdot}20$) the Kagomé net of occupied Ba^{2+} sites common to the $x = 0{\cdot}8$ and $x = 1{\cdot}2$ structures. This range of composition may then be explained by the gradual insertion of additional Ba^{2+} ions into the central pair of sites as indicated in Fig. 7. (The situation is further complicated, however, by a simultaneous variation in the mean spacing between $m = 2$ type intergrowths, which results in a continuous variation in m for $4{\cdot}70 < m < 5{\cdot}0$, Possible energetic origins for the latter are discussed in §6.) The existence of this partially filled

pair of sites for $0{\cdot}8 < x < 1{\cdot}20$ is entirely consistent with the dielectric absorption measurements of Dryden & Wadsley. These indicate only one activation energy (0·17 eV) for Ba^{2+} ions hopping throughout this stoichiometry range. Our observations and analysis immediately suggest that this common hopping process is simply exchange of Ba^{2+} in the central pair of sites located within a relatively stable honeycomb-like framework of Ba^{2+} ions. The activation energy for this process will be independent of x, to first order, as observed. It is interesting to note that it is not rows of the c-axis tunnel sites which empty as x decreases, rather there are short rows ($\lesssim$60 Å) of empty tunnel sites aligned along [100].

The intuitively attractive structure expected for $x = 1$, *i.e.* the Ba^{2+}–vacancy–Ba^{2+}–vacancy model of Dryden & Wadsley, occurs only in the form of small elements of $m = 2$ intergrown with $m = 5$ structure. Thus for $x = 1{\cdot}0$ we find $m = 4{\cdot}81$ (Fig. 4*b*). This is achieved by mixing the $m = 5$ structure ($0{\cdot}8 < x < 1{\cdot}2$, $x = 1{\cdot}0$) with $m = 2$ ($x = 1{\cdot}0$) elements. Again a microdomain texture is observed, as indicated in Fig. 4(*c*).

For $x > 1{\cdot}20$ the multiplicity m continues to increase continuously from 5 to towards 6. In fact the upper limit found so far is 5·93. The image shown in Fig. 4(*d*) shows domains of a new pattern of white blobs which lead to the structural model shown in Fig. 8(*a*). This has stoichiometry $x = 1{\cdot}33$ and apparently it is this structure which intergrows with $m = 5$ in the interval $1{\cdot}2 < x < 1{\cdot}33$. Note that the unit cell is not body-centred in this case, unlike all of the cells shown for the $m = 5$ and $m = 2$ structures. It contains a zigzag arrangement of vacant sites along [010], in common with $m = 5$, $x = 1{\cdot}2$, but these are separated by *pairs* of filled Ba^{2+} sites to give periodicity $6 \times d_{002}$ in reciprocal space. Again it is necessary to invoke a microdomain model, with irregular intergrowths of $m = 5$ and $m = 6$ structures (Fig. 8*b*), to explain the continuous variation of m observed for $1{\cdot}2 < x < 1{\cdot}33$. More detailed calculations of the continuous variation of position of the superlattice peaks with composition, and of their intensity, are in preparation. This analysis uses the

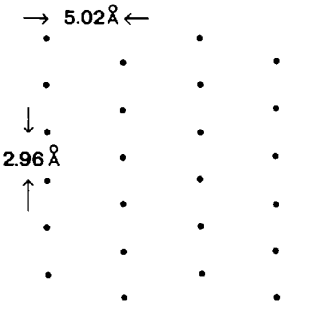

Fig. 5. Pattern of ideal Ba^{2+} sites in the [100] projection of hollandite.

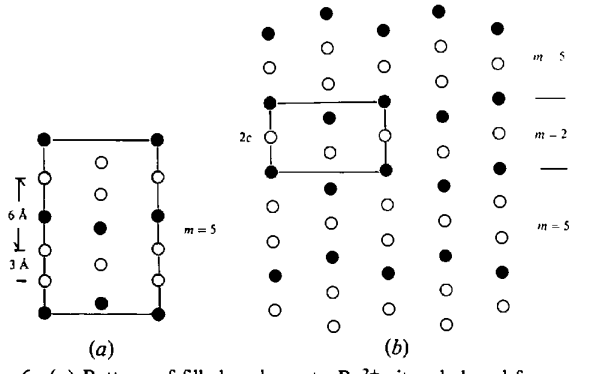

Fig. 6. (*a*) Pattern of filled and empty Ba^{2+} sites deduced for $x = 0{\cdot}8$ by a study of Fig. 4(*a*). Note the 6 and 3 Å empty-site spacings along [001]. (*b*) Intergrowth of $m = 5$ and $m = 2$ structures deduced from Fig. 4(*a*) showing sequence changes required to give mean multiplicity of $m = 4{\cdot}75$ rather than $m = 5$.

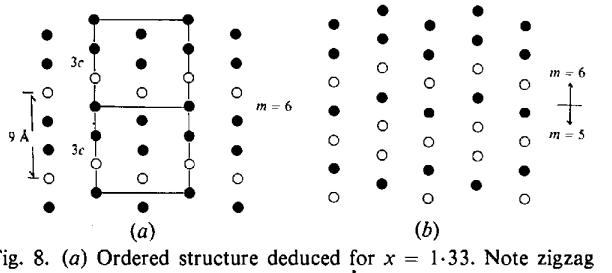

Fig. 8. (*a*) Ordered structure deduced for $x = 1{\cdot}33$. Note zigzag arrangement of empty sites having 9 Å ($m = 6$) periodicity along [001]. (*b*) Intergrowth of $m = 6$ and $m = 5$ structures required to explain continuous variation of m and x in the stoichiometry range $1{\cdot}2 < x < 1{\cdot}33$ ($5 < m < 6$).

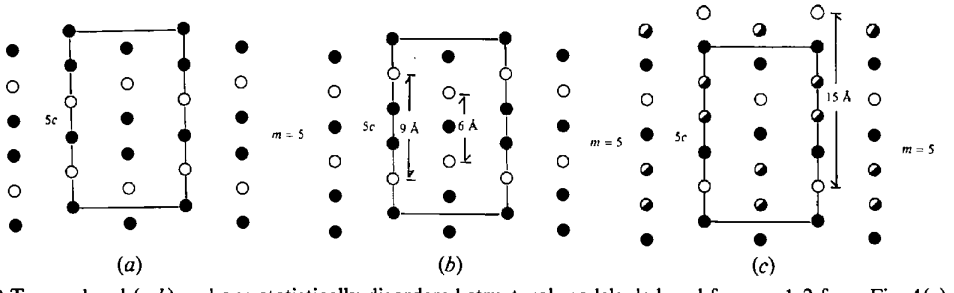

Fig. 7. (*a*),(*b*),(*c*) Two ordered (*a*,*b*) and one statistically disordered structural models deduced for $x = 1{\cdot}2$ from Fig. 4(*c*). Note the 6 and 2 Å empty-site spacings along [001].

principles already applied successfully to explain the variation of intensity and spacing of the incommensurate superlattice observed for iron-doped rutiles (Grey & Bursill, 1978).

It appears that for the Ba/Mg and Ba/Ga hollandites the upper limit of x is just slightly less than 1·33 (corresponding to $m = 5{\cdot}93$). This should be compared to the range $1{\cdot}54 < x < 2{\cdot}0$ observed for the K/Al hollandites by Beyeler.

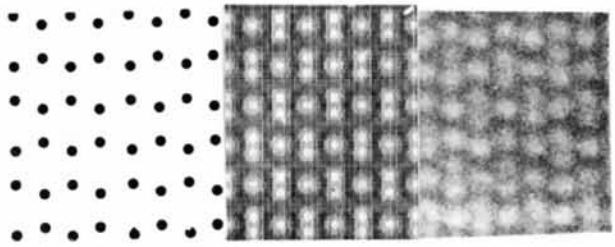

(*a*) (*b*) (*c*)

Fig. 9. (*a*) Structural model, (*b*) computed image and (*c*) experimental image for $x = 0{\cdot}8$.

5. Computer simulation of the images

The atomic coordinates for the structural models derived above were calculated and used for computer simulation of the images, using techniques described previously (MacLagan, Bursill & Spargo, 1977; Bursill & Wilson, 1977).

(*a*) $m = 5, x = 0{\cdot}8$

Fig. 9(*a*,*b*,*c*) compares the structural model and the computer-simulated and experimental images corresponding to $Ba_{0{\cdot}8}Mg_{0{\cdot}8}Ti_{7{\cdot}2}O_{16}$. The electron-optical parameters obtained are $H = 60$ Å, $\Delta f = -600$ Å and effective resolution $R = 2{\cdot}8$ Å. Good agreement is obtained. We note, however, that the computed through-focal series of images (Fig. 10) clearly did not show the behaviour predicted by the PCDA; thus there is no zero-contrast condition and no simple reversal of contrast on going through-focus. The computed images do show a good one-to-one correspondence between white-blob position and the empty Ba^{2+} sites in the model for $-600 < \Delta f < -500$ Å for thickness $20 < H$

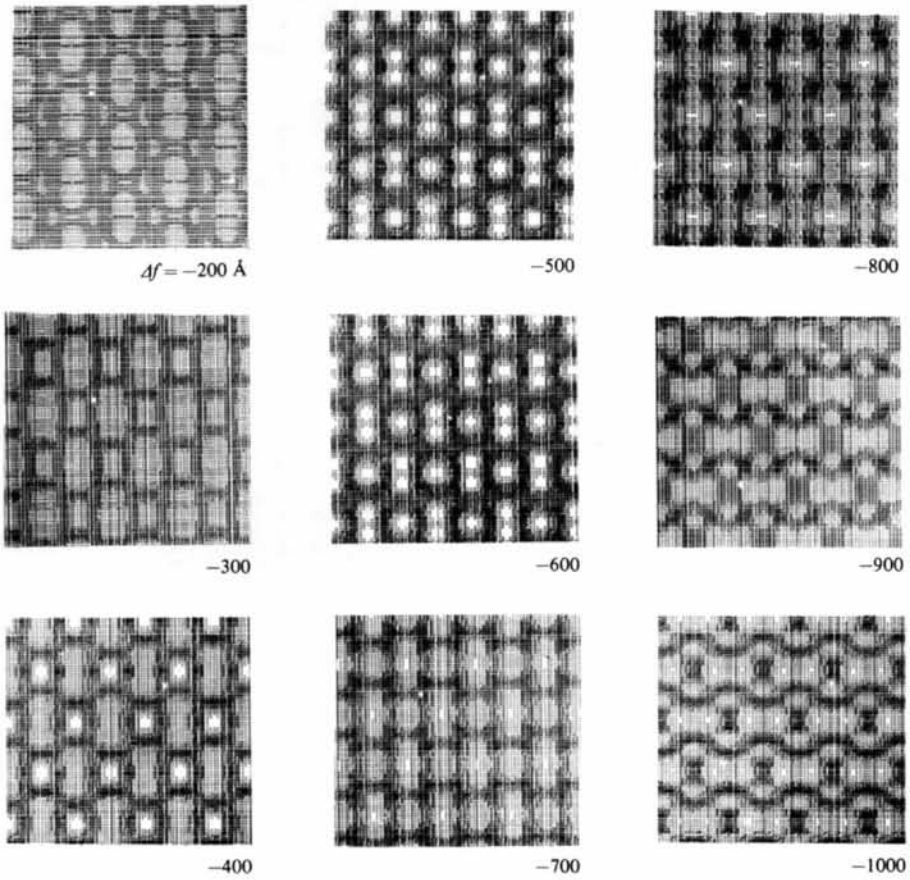

Fig. 10. Part of through-focal series of computed images for an $x = 0{\cdot}8$ ($m = 5$) structure showing the appearance of an interpretable image for $-600 < \Delta f < -500$ Å ($H = 60$ Å).

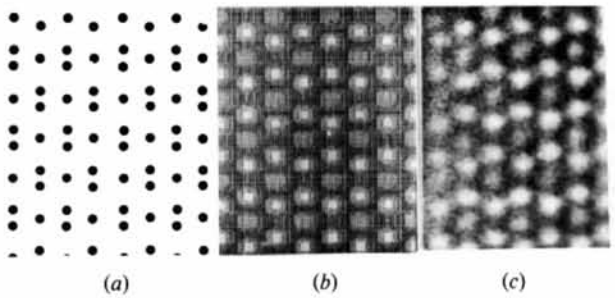

(*a*) (*b*) (*c*)

Fig. 11. (*a*) Structural model, (*b*) computed image and (*c*) experimental image for $x = 1{\cdot}20$.

< 100 Å or even more. Thus the image is interpretable in the sense of being able to locate the empty sites and, furthermore, this image is stable over a significant range of electron-optical parameters. However, it is important to note that the blob spacing corresponding to the pair of empty sites at the centre of the honeycomb structure varies considerably with Δf and H, *i.e.* from approximately 2·7 to 3·2 Å in the above range of values of Δf and H. Thus it is not possible to measure the displacement parameter u introduced by Beyeler to describe the effects of repulsion between Ba^{2+} ions. Precise values of C_s, Δf and H are required for such an analysis and at present the experimental errors involved in measuring all three of these are far too great (~10%) to allow this type of analysis to be seriously considered. Thus displacements as large as the 0·71 Å proposed for K^+ by Beyeler are not inconsistent with the images.

(*b*) $m = 5, x = 1{\cdot}2$

Fig. 11(*a*,*b*,*c*) compares the model and the computed and observed images corresponding to $Ba_{1\cdot2}Mg_{1\cdot2}Ti_{6\cdot8}O_{16}$. The image match was obtained for $\Delta f = -600$ Å, $H = 60$ Å but in this case the defocus setting required to retain a one-to-one correspondence with the empty Ba^{2+} sites is less critical ($-650 < \Delta f < -400$ Å).

Fig. 12(*a*,*b*) compares through-focal series for $H = 60$ Å of the ordered and disordered models shown in Fig. 7(*a*,*c*). Note that these may be easily distinguished by noting that the ordered structure shows 6 and 9 Å white-blob spacings whereas the disordered structure shows only 15 Å blob spacings along *c*. Both of these types of contrast have been found in the experimental images.

(*c*) $m = 6, x = 1{\cdot}33$

Fig. 13(*a*,*b*,*c*) compares the structural model and the computed and observed images corresponding to $Ba_{1\cdot33}Mg_{1\cdot33}Ti_{6\cdot67}O_{16}$. In this case the white-blob spacing is always 9 Å and the interpretable image occurs over a narrower range of Δf values, *i.e.* $-600 \leq \Delta f \leq 450$ Å.

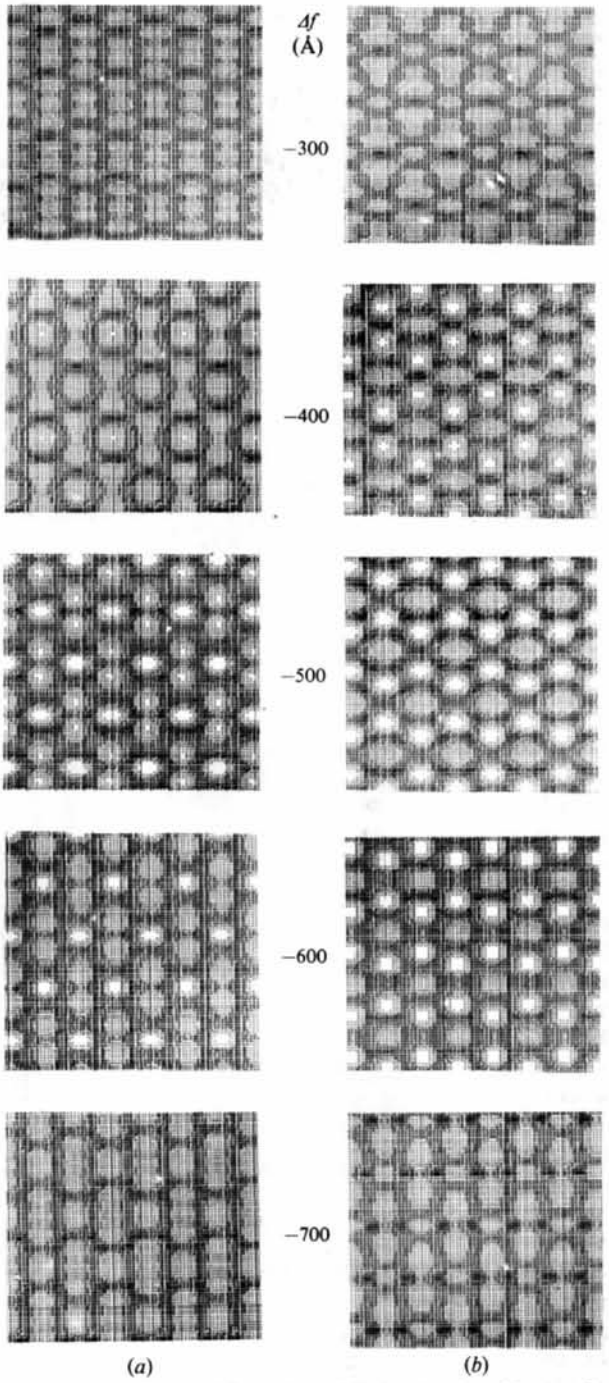

(*a*) (*b*)

Fig. 12. Comparison of part of through-focal series of images for ordered and disordered structural models (*cf.* Fig. 7*a*,*c* respectively) of $x = 1{\cdot}20$ ($m = 5$) for crystal thickness $H = 60$ Å. Note that 6 and 9 Å blob spacings predominate along tunnels in (*a*), whereas only 15 Å spacings dominate in (*b*).

The experimental images show many variations in contrast apart from the examples discussed above. These may be due to overlapping of short-range-ordered domains along the projection axis and the

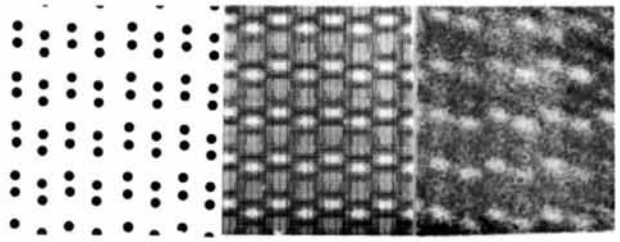

(a) (b) (c)

Fig. 13. (a) Structural model, (b) computed image and (c) experimental image for $x = 1{\cdot}33$.

details of the intergrowth sequences required to explain the non-integral superlattice spacings. A more detailed discusssion of the defect or intergrowth structures must be left for a later paper. However, the good agreement between the computer-simulated images for $x = 0{\cdot}8$, $1{\cdot}2$ and $1{\cdot}33$ for selected relatively well ordered areas does establish the nature of the basic structures involved.

6. Discussion

The most striking result of the present study is the relatively narrow range of superlattice spacings observed, corresponding to $4{\cdot}75 < m < 5{\cdot}93$. Thus the intuitively simple $m = 2$ structure corresponding to $x = 1{\cdot}0$ is almost completely avoided, although it does play an important role in providing a structural mechanism which allows m to vary continuously from 4·75 to 5·93. Whilst it is clear that Ba–Ba electrostatic interactions will naturally lead to short- or long-range-order correlations one would expect the simple Ba^{2+}–vacancy–Ba^{2+}–vacancy sequence to occur for $x = 1{\cdot}0$. We therefore must consider that the superlattice period may also be determined by some property of the supposedly rigid MX framework. Inelastic neutron diffraction studies of the phonon spectra of rutile show a pronounced inflection in the Λ_5 transverse acoustical mode for $k_{001} = 0{\cdot}33$ (Traylor, Smith, Nicklow & Wilkinson, 1971). One might anticipate that this will result in a tendency for superlattice formation in the rutile structure with multiplicity $6 \times d_{002}$ and, in fact, many so-called trirutiles do occur in mineralogy having just this periodicity (*i.e.* $3c$); see, for example, Brandt (1943). We note that the hollandite framework may be derived from rutile by selecting columns having a cross section consisting of four corner-shared octahedra and elongated parallel to c_r and rotating these cooperatively as shown in Fig. 14. We suggest, therefore, that the same Λ_5 vibration mode propagating along $c_{rut} \equiv c_{holl}$ will remain in the hollandite structure and it is a softening of this mode which imposes the superlattice periodicity on the tunnel structure. The precise multiplicity of the softening mode will not be the same as it is

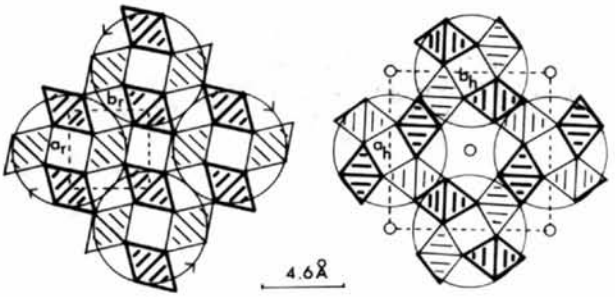

(a) (b)

Fig. 14. Structural relationship between rutile and hollandite. In rutile (a) (MO_6) octahedra share edges along the projection axis $[001]_r$; these are linked by corner-sharing only in the plane of projection. Note the corresponding rutile-like columns (circled) in the hollandite structure (b). Rotation of such columns by $\pi/4$ rad, alternately clockwise and anticlockwise, generates hollandite.

in pure rutile since the rutile-like columns are linked together in a different way, giving edge-sharing around the tunnels. The force constants of the hollandite framework will also depend on the amount of Ti^{4+} which has been substituted by Mg^{2+} (or Ga^{3+}). Thus the superlattice repeat may well increase from $3c$ to $\sim 5c$, with variations in the range $4{\cdot}75c \leq 5c \leq 5{\cdot}93c$, depending upon the Mg/Ti ratio in the framework. Further evidence for the importance of this ratio is provided by the stability range observed for the K hollandites $K_{2x}Mg_xTi_{8-x}O_{16}$ ($0{\cdot}75 < x < 1{\cdot}0$). The onset of this phase occurs for $x = 0{\cdot}75$ when Mg/Ti = 0·103, compared with the corresponding value for $Ba_xMg_xTi_{8-x}O_{16}$ ($0{\cdot}18 < x < 1{\cdot}33$) which is Mg/Ti = 0·111. The maximum x value for the K hollandite is limited to $x = 1{\cdot}0$, when all of the cubic coordinated sites in the tunnel are filled. Thus the range of Mg/Ti ratios does correspond very closely in the two phases.

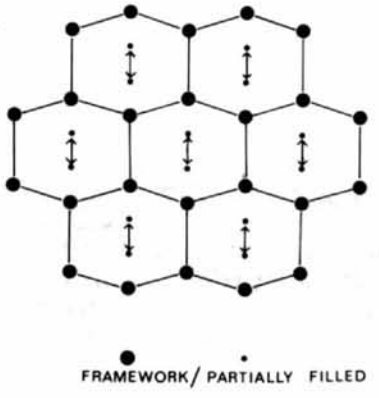

Fig. 15. Honeycomb ($m = 5$) framework of filled Ba^{2+} sites showing the central pair of sites which are partially occupied in the composition range $0{\cdot}8 < x < 1{\cdot}20$. Exchange of Ba^{2+} ions (arrowed) between these sites may explain dielectric absorption results indicating Ba^{2+} ion hopping with an activation energy 0·17 eV.

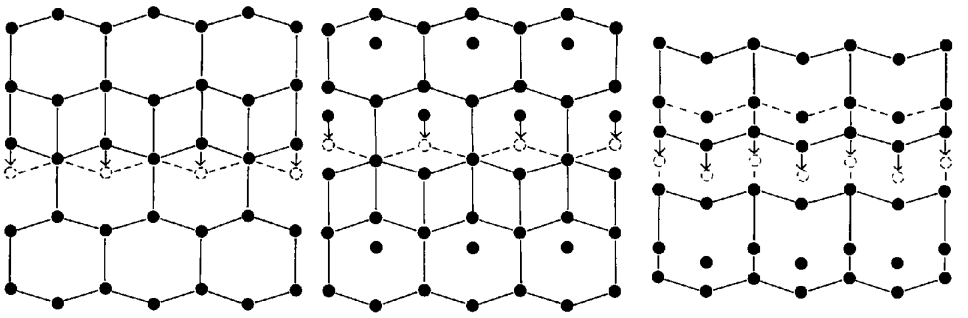

Fig. 16. (*a*) Cooperative diffusion of Ba^{2+} ions allowing movement of the $m = 2$ structural elements in a crystal having, for example, $x = 0{\cdot}8$, $m = 4{\cdot}75$. The $m = 2$ regions need not extend more than one or two unit cells along [010], giving rise to an irregular stepwise intergrowth of $m = 5$ and $m = 2$. (*b*) Cooperative diffusion in the $x = 1{\cdot}20$, $m = 5$ structure, consisting of movement of antiphase domain boundaries between the ordered structures shown in Fig. 7(*a*,*b*). Again correlations along [010] are expected to be short (~10–20 Å). (*c*) Cooperative diffusion of Ba^{2+} ions in the $x = 1{\cdot}33$ ($m = 6$) structure. As with (*a*) and (*b*), strong electrostatic repulsions will tend to re-establish short-range order during the diffusion process.

The incommensurate superlattice periodicity $4{\cdot}55c$ found by Beyeler for $K_{1{\cdot}54}Mg_{0{\cdot}77}Ti_{7{\cdot}23}O_{16}$ lies close to the range found for the Ba hollandites. Our own preliminary diffraction studies of $K_{2x}Mg_xTi_{8-x}O_{16}$ have revealed periodicities $4{\cdot}1c \leq 5c \leq 6{\cdot}6c$ for $1{\cdot}50 \leq x \leq 1{\cdot}80$. Lattice-image studies of these phases are also in progress. However, in this case the superlattice peaks are diffuse, as observed by Beyeler, and the short-range-ordered domain structure will be more difficult to interpret. It is also significant that the total positive-ion charge density in the tunnels also ranges over approximately the same limits for the K^+ and Ba^{2+} hollandite phases. It may therefore be argued that it is primarily the positive charge in the tunnels which stabilizes the tunnel structure. Cohesive-energy calculations and inelastic neutron diffraction studies are planned to resolve this question. [We have previously established an excellent correlation between the incommensurate periodicities observed in the ion-doped rutiles $Fe_2Ti_{n-2}O_{2n-1}$ ($20 < n < 30$) and the marked discontinuity in the Δ_3 acoustic mode of rutile for $k_{010} = 0{\cdot}22$ (see Bursill & Grey, 1979; Netherway, Bursill & Wood, 1979).]

It is important to note that if the superlattice period is non-integral (*i.e.* incommensurate with the lattice) then the intergrowth structures required to attain this spacing must of necessity be irregular rather than ordered. Thus, for $m = 4{\cdot}70$ we intergrow $m = 5$ and $m = 2$ structures in the ratio 9 : 1. Rather than form an ordered structure having periodicity $47c$ (*i.e.* 141 Å) we find an irregular intergrowth having mean period $4{\cdot}70c$. This provides further support for the idea that the periodicity is imposed by the force constants of the MX_2 framework and is not simply due to electrostatic repulsions between relatively free Ba^{2+} ions in the tunnels. The latter would tend to produce a regular or uniform distribution.

The presence of ordered domains within the hollandite structure and the admixture with $m = 2$ structure elements provides a structural explanation for the disappointing lack of success of hollandite phases as fast-ion conductors. The relatively rigid honeycomb arrangement of Ba^{2+} ions imposes an unexpected activation-energy barrier opposing diffusion in the tunnels. Thus even though the dielectric measurements yielded a low activation energy (0·17 eV) for Ba^{2+} ions hopping in the tunnels it is now clear that this measurement refers to exchange of the central pair of sites with the honeycomb framework (see Fig. 15). In order to have bulk diffusion of Ba^{2+} ions in hollandite it is necessary to have concerted movements of Ba^{2+} ions closely resembling domain-boundary diffusion, as indicated for $m = 0$, 8, 1·2 and 1·33 intergrowth structures in Fig. 16(*a*,*b*,*c*). Further direct studies of the diffusion mechanism may be possible using a high-temperature stage in the electron microscope.

In view of the above results it now appears to us that the suggested use of a mixed Ba/Cs hollandite phase as a depository of radioactive Cs (Ringwood, 1978) is worthy of further investigation. As pointed out by Ringwood, natural hollandite minerals do appear to be stable on a geological time scale.

This work was financially supported by the Australian Research Grants Committee and the University of Melbourne.

References

BEYELER, H. (1976). *Phys. Rev. Lett.* **37**, 1557–1560.

BOYCE, J. B. & HUBERMAN, B. A. (1979). *Phys. Rep.* **15**, 189–265.

BRANDT, K. (1943). *Ark. Kemi Mineral. Geol.* **17A**(6), 17.

BURSILL, L. A. (1979*a*). *Acta Cryst.* B**35**, 530–538.
BURSILL, L. A. (1979*b*). *Acta Cryst.* A**35**, 449–458.
BURSILL, L. A. (1979*c*). *Direct Imaging of Atoms in Crystals and Molecules.* Nobel Symp. No. 47, Lidingo; *Chem. Scr.* **14**, 83–97.
BURSILL, L. A. (1980). *Acta Cryst.* B**36**, 2897–2902
BURSILL, L. A. & GREY, I. E. (1979). *Modulated Structures* 1979, Kailua-Kona, Hawaii, edited by J. M. COWLEY, Conf. Proc. No. 53, pp. 364–366. New York: American Institute of Physics.
BURSILL, L. A., SPARGO, A. E. C., WENTWORTH, D. & WOOD, G. J. (1979). *J. Appl. Cryst.* **12**, 279–286.
BURSILL, L. A. & WILSON, A. R. (1977). *Acta Cryst.* A**33**, 672–676.
BURSILL, L. A. & WOOD, G. J. (1978). *Philos. Mag.* **38**, 673–689.
BYSTRÖM, A. & BYSTRÖM, A. M. (1950). *Acta Cryst.* **3**, 146–154.
DRYDEN, J. S. & WADSLEY, A. D. (1958). *Trans. Faraday Soc.* **54**, 1574–1580.
GREY, I. E. & BURSILL, L. A. (1978). *Acta Cryst.* B**34**, 2412–2424.
LYNCH, D. F., MOODIE, A. F. & O'KEEFE, M. A. (1975). *Acta Cryst.* A**31**, 300–307.
MACLAGAN, D. S., BURSILL, L. A. & SPARGO, A. E. C. (1977). *Philos. Mag.* **35**, 757–780.
NETHERWAY, D. J., BURSILL, L. A. & WOOD, G. J. (1979). *Modulated Structures* 1979, Kailua-Kona, Hawaii, edited by J. M. COWLEY, Conf. Proc. No. 53, pp. 162–164. New York: American Institute of Physics.
REAN, J.-M., DELMAS, C. & HAGENMULLER, P. (1978). *Solid Electrolytes*, edited by P. HAGENMULLER & W. VAN GOOL, pp. 381–391. New York: Academic Press.
RINGWOOD, A. E. (1978). *Safe Disposal of High-Level Nuclear-Reactor Wastes: A New Strategy*, pp. 26–45. Canberra: Australian National Univ. Press.
TRAYLOR, J. G., SMITH, H. G., NICKLOW, R. M. & WILKINSON, M. K. (1971). *Phys. Rev. B*, **3**, 3457–3472.

Acta Cryst. (1980). B**36**, 2913–2918

The Structure and Chemistry of a Barium Titanate Hollandite-Type Phase

BY W. SINCLAIR

Research School of Earth Sciences, Australian National University, PO Box 4, *Canberra, ACT* 2600, *Australia*

G. M. MCLAUGHLIN

Research School of Chemistry, Australian National University, PO Box 4, *Canberra, ACT* 2600, *Australia*

AND A. E. RINGWOOD

Research School of Earth Sciences, Australian National University, PO Box 4, *Canberra, ACT* 2600, *Australia*

(*Received* 26 *October* 1979; *accepted* 2 *September* 1980)

Abstract

The crystal structure of a synthetic hollandite phase $(Ba_{0.98}Ca_{0.03}Zr_{0.02})(Al_{1.10}Ni_{0.48}Ti_{6.4})O_{16}$ has been refined by the full-matrix least-squares method using 624 three-dimensional reflections to a final R value of 0·059 for the 22 variables involved. The data were collected on a four-circle diffractometer using graphite-monochromated Mo $K\alpha$ radiation. The structure is tetragonal, space group $I4/m$ with cell dimensions a = 10·039 (1), c = 2·943 (1) Å, and Z = 2. Refinement of the structure with the large A cations on the 2(b) site (0,0,½) resulted in an unacceptably high residual. This atom was displaced to site 4(e) (0,0,±z) with z = 0·3845 (7), as indicated by the difference electron density map, and refinement proceeded satisfactorily. There are now two A—O(1) bond distances, four each of 2·787 (3) and 3·126 (3) Å. The O(1) atoms form a cage-like framework around the 4(e) site which effectively immobilizes large A atoms such as Cs, K, Rb and Ba. Results of solid-state preparations of $Ba_xAl_{2x}Ti_{8-2x}O_{16}$ show a large range of x, varying from 0·3–1·2.

Introduction

$BaAl_2Ti_6O_{16}$ (ideal formula) is the most abundant phase used in SYNROC, a synthetic rock developed for nuclear-waste immobilization (Ringwood, 1978). This synthetic phase possesses the tetragonal hollandite structure and is capable of a large number of

0567-7408/80/122913-06$01.00